Applied Physics Letters

Perspectives on MOVPE-grown (100) β-Ga_2O_3 thin films and its Al-alloy for power electronics application

Cite as: Appl. Phys. Lett. **121**, 240503 (2022); https://doi.org/10.1063/5.0122886
Submitted: 26 August 2022 • Accepted: 29 November 2022 • Published Online: 14 December 2022

Jana Rehm, Ta-Shun Chou, Saud Bin Anooz, et al.

Applied Physics Letters PERSPECTIVE scitation.org/journal/apl

Perspectives on MOVPE-grown (100) β-Ga_2O_3 thin films and its Al-alloy for power electronics application

Cite as: Appl. Phys. Lett. **121**, 240503 (2022); doi: 10.1063/5.0122886
Submitted: 26 August 2022 · Accepted: 29 November 2022 ·
Published Online: 14 December 2022

Jana Rehm,[a] Ta-Shun Chou, Saud Bin Anooz, Palvan Seyidov, Andreas Fiedler, Zbigniew Galazka, and Andreas Popp

AFFILIATIONS

Leibniz-Institut für Kristallzüchtung (IKZ), Max-Born-Str., 2, 12489 Berlin, Germany

[a]Author to whom correspondence should be addressed: jana.rehm@ikz-berlin.de

ABSTRACT

Beta gallium oxide (β-Ga_2O_3) is a promising ultra-wide bandgap semiconductor with attractive physical properties for next-generation high-power devices, radio frequency electronics, and solar-blind ultraviolet radiation detectors. Here, we present an overview and perspective on the development of MOVPE-grown (100) β-Ga_2O_3 thin films and its role in supplementing high-power electronics. We review the development path of the growth process on (100) β-Ga_2O_3 thin films with a discussion regarding the solved and remaining challenges. The structural defect formation mechanism, substrate treatment strategies, and different growth windows are analyzed to optimize the grown film to fulfill the requirements for device fabrication. Toward industrial applications, MOVPE-grown β-Ga_2O_3 thin films are evaluated in two aspects: thick layers with smooth surface roughness and the electrical properties in terms of high carrier mobility and low doping concentration. Based on the reviewed results, we propose strategies in substrate preparation treatments and supportive tools such as the machine learning approaches for future growth process optimization and envision the rising interest of the β-Ga_2O_3-related alloy, β-$(Al_xGa_{1-x})_2O_3$.

INTRODUCTION

The constant development of our modern society and the resulting increase in the combustion of fossil fuels to meet the world's energy demand has left unprecedented marks on the Earth's environment. Utilizing high-efficiency power electronics in a wide range of fields such as energy saving, energy storage, renewable energy systems, and electric vehicles will have a tremendous contribution to the decarbonization of the global energy sector, hence, mitigating the effects of global warming and enabling the development toward a sustainable society.[1] Starting with the introduction of the first transistor in the 1940s, the power electronics market was dominated by Si-based devices finding their application in various fields, including power switching, radio frequency (RF), communication systems, and optoelectronics.[1–4] However, owing to its intrinsic material characteristics, Si-based technology nowadays approaches its theoretical performance limitations in terms of efficient high-power and high-voltage devices,[3,5] which are urgently needed to meet the increasing demand for sustainable power generation and conversion. Wide bandgap semiconductors such as 4H-SiC and GaN offer superior material properties compared to conventional Si-based power devices due to their much larger bandgap energy (3.3 and 3.4 eV, respectively[6]) and higher breakdown electric fields, thus, allowing to realize power switching devices with increased power densities and overall better performances.[4,6–8] Although 4H-SiC- and GaN-based power electronics are already commercially available, the lack of low-cost native single crystal substrates[9] still remains a major drawback for large-scale industrial production and utilization. Over the past decade, β-Ga_2O_3 emerged as a promising candidate for next-generation high-power and high-frequency applications beyond 4H-SiC and GaN.[10] Owing to its ultra-wide bandgap of approximately 4.5–4.9 eV (Ref. 8) and a high theoretical breakdown field strength of about 7–8 MV cm^{-1},[8] β-Ga_2O_3 exhibits an up to ten-times higher Baliga's figure-of-merit (BFOM) than 4H-SiC and an up to four-times higher BFOM than GaN[6] and, therefore, shows great potential to outperform its already established technological counterparts. The high estimated breakdown field allows for a more compact design with miniatured device dimensions and a reduced minimum thickness of the low/medium-doped drift layer which leads to a low to low on-resistance and reduced switching losses in high-power devices. Furthermore, the availability of β-Ga_2O_3 high-quality single crystal substrates grown by

various melt growth techniques such as Czochralski,[11,12] edge-defined film-fed growth (EFG),[13] and vertical Bridgman technique (VB)[14,15] allows for homoepitaxial growth and future mass production of β-Ga_2O_3 based high-power devices at low cost.

The excellent intrinsic material properties of β-Ga_2O_3 can be integrated into a lateral or vertical device architecture, where both variants come with their specific application fields and requirements, including high-voltage switching devices, solar-blind ultraviolet (UV) photodetectors, or gas sensors, and can potentially be further implemented into systems operating at even harsh-environmental conditions.[3,4,8,16–18] A comprehensive overview of typical device designs for β-Ga_2O_3-based lateral and vertical power devices is illustrated in Fig. 1.

Device architectures

In general, lateral and vertical β-Ga_2O_3-based power devices necessitate homoepitaxial drift layers exhibiting smooth surface morphologies and high crystalline qualities with a low intrinsic defect density and negligible acceptor compensation. Homoepitaxial growth is advantageous since it allows to grow layers without lattice mismatch and maintains a high structural perfection over varying layer thicknesses.

The lateral device architecture consists of a medium to highly n-doped (10^{17}–10^{19} cm^{-3}) 200–300 nm thick β-Ga_2O_3 channel, exhibiting a sharp interface to the semi-insulating substrate. It is preferentially utilized in low to medium voltage (<600 V, 600 V, 1.2 kV) devices such as power switches, RF switches, power suppliers, or power amplifiers. The successful fabrication of lateral β-Ga_2O_3 metal–oxide–semiconductor field effect transistors (MOSFETs) and Schottky junction metal–semiconductor field effect transistors (MESFETs) has already been demonstrated by several research groups.[19–23] To fully exploit the theoretical high breakdown field strength of β-Ga_2O_3, a vertical device architecture targeting its application in the medium to high (1.2–6 kV) and ultra-high-voltage regime (>6 kV) is preferable. In contrast to lateral devices, where a large area β-Ga_2O_3 drift layer is required to withstand high-voltage applications, vertical high-power β-Ga_2O_3 devices with high blocking voltages can be fabricated by increasing the epitaxial layer thickness, which offers a better chip area utilization and up-scaling potential. Vertical high-power β-Ga_2O_3 devices necessitate homoepitaxial ultra-low doped (<10^{16} cm^{-3}) drift layers with thicknesses ranging between several to several tens of micrometers, which are grown on a conductive substrate at reasonable growth rates (>1 $\mu m\,h^{-1}$). Punch-through designs targeting the ultra-high-voltage regime (e.g., 10 kV) require an approximately 17 μm thick drift layer with a max. doping concentration of mid 10^{15} cm^{-3} when an average breakdown field strength of 6 MV cm^{-1} is estimated. Triangular device structures reaching the max. theoretical surface breakdown electric field of 8 MV cm^{-1} necessitate a drift layer of 25 μm with a low 10^{16} cm^{-3} doping concentration. In general, punch-through breakdown characteristics in vertical β-Ga_2O_3 devices are favorable over triangular structures, since they allow to maximize the average electric field over the entire drift region, thus, fully utilizing the potential of the ultra-wide bandgap material. MOVPE-grown (010)-β-Ga_2O_3 based vertical field plate Schottky barrier diodes exhibiting an average punch-trough breakdown electric field of 2.29 MV cm^{-1} has been reported.[24] Utilizing a vertical dielectric heterojunction structure by integrating a high permittivity dielectric field oxide with n-type β-Ga_2O_3, a record high electric field of 5.7 MV cm^{-1} has been demonstrated by Xia *et al.*[25] Although the $BaTiO_3$/β-Ga_2O_3 diodes consisted of relatively thin drift regions (150 nm unintentionally doped β-Ga_2O_3) and the resulting breakdown voltage of 85 V has not reached the regime for ultra-high-voltage applications yet, the integration of improved design and field management strategies provide a basis for future β-Ga_2O_3 vertical devices with thicker epitaxial layers and higher breakdown voltages. To achieve the necessitated layer thicknesses of several to several tens of micrometers and maintain a high material quality over such large layer dimensions, a profound understanding of how different growth parameters such as chamber pressure, temperature, and VI/III ratio affect the surface morphology and structure of the β-Ga_2O_3 layer is required. Especially in the low doping regime (<10^{16} cm^{-3}), a precise control of the highly process-dependent incorporation of impurities during the epitaxial growth is indispensable.

β-$(Al_xGa_{1-x})_2O_3$ alloys

Increasing the bandgap by alloying β-Ga_2O_3 with Al_2O_3 opens up the possibility of realizing the fabrication of lateral β-$(Al_xGa_{1-x})_2O_3$/β-Ga_2O_3 heterostructure modulation-doped field effect

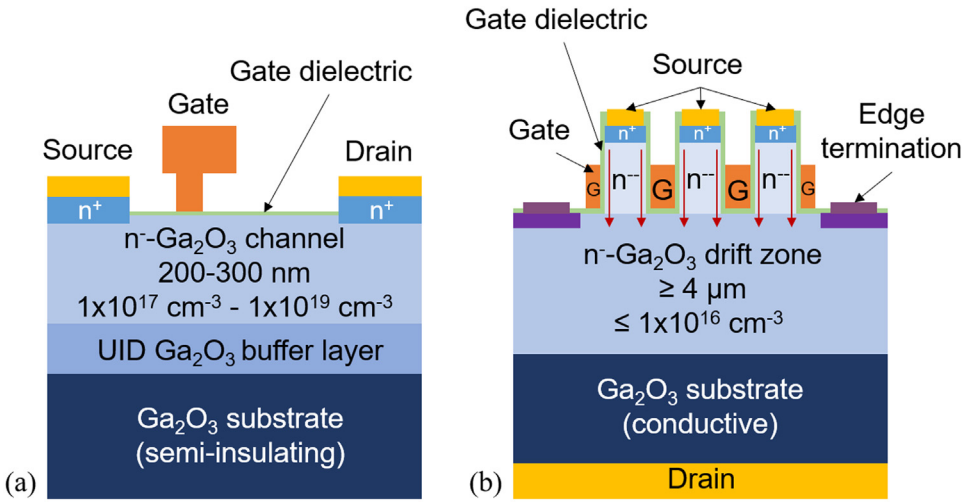

FIG. 1. Illustration of typical designs for β-Ga_2O_3-based lateral (a) and vertical power devices (b).

transistors (MODFETs),[26–29] which are predicted to show a significant enhancement in the device performance compared to β-Ga_2O_3 based devices.[30] In contrast to uniformly doped β-Ga_2O_3 thin films, where room-temperature mobilities are limited to 200 $cm^2\ V^{-1}\ s^{-1}$ (Ref. 31) by enhanced polar optical phonon scattering, in modulation-doped barrier layers with sharp doping profiles, higher electron mobilities can be realized due to the reduction of scattering events resulting from the separation of the two-dimensional electron gas (2DEG) channel from ionized donor impurities.[26,28,29,32,33] To maximize the performance of modulation-doped β-$(Al_xGa_{1-x})_2O_3/Ga_2O_3$ heterostructure devices, the development of high-quality β-$(Al_xGa_{1-x})_2O_3$ epitaxial films with high Al compositions resulting in large band offsets at the β-$(Al_xGa_{1-x})_2O_3/Ga_2O_3$ interface is required.[33,34]

The material properties for β-Ga_2O_3 and β-$(Al_xGa_{1-x})_2O_3$ alloys with $x = 0.25$ and $x = 0.5$, respectively, are summarized in Table I. Duan *et al.*[37] calculated that the electron mobility for ordered β-$(Al_{0.25}Ga_{0.75})_2O_3$ and β-$(Al_{0.5}Ga_{0.5})_2O_3$ alloys at 300 K is limited to approximately 104 and 81 $cm^2\ V^{-1}\ s^{-1}$, respectively, due to enlarged Pauling ionicity, Fröhlich coupling constant, and optical phonon scattering as the Al composition increases. The results imply that, indeed, at least 30% to 35% Al content in homogenously doped β-$(Al_xGa_{1-x})_2O_3$ alloys is required to result in a BFOM equivalent to β-Ga_2O_3, but with a significantly larger breakdown field strength by $\sim$2 MV cm^{-1} due to the wider bandgap. However, Varley[40] predicted BFOM values for β-$(Al_xGa_{1-x})_2O_3$ as a function of Al composition with various model mobilities ranging from constant to β-Ga_2O_3 to rapidly decreasing with higher Al contents, showing that if the mobility can be maintained relative to β-Ga_2O_3, the resulting BFOM for a variety of compositions should exceed that of β-Ga_2O_3. Since only a few experimental studies have been published yet regarding homogenous doping of β-$(Al_xGa_{1-x})_2O_3$ layers with varying Al compositions,[30,42,43] and the growth of high-quality films without phase segregation or degradation of the crystalline quality at high Al compositions on β-Ga_2O_3 substrates is still challenging,[30,32–34,42,44–47] the potential of β-$(Al_xGa_{1-x})_2O_3/Ga_2O_3$ heterostructures remains to be explored and clarified. Moreover, due to the lattice mismatch between the β-$(Al_xGa_{1-x})_2O_3$ layer and the β-Ga_2O_3 substrate, heteroepitaxial growth beyond a critical thickness will lead to an enhanced formation of dislocations in the layer as a consequence of strain release and, therefore, to a degradation of the thin-film quality. Homoepitaxial growth will allow us to maintain a higher crystalline quality over a wide range of Al compositions and layer thicknesses, and, therefore, is urgently needed. A β-$(Al_xGa_{1-x})_2O_3$ bulk crystal growth study with up to 30% Al composition and the corresponding electrical properties is soon to be published by Zbigniew Galazka *et al.* from the Leibniz-Institut für Kristallzüchtung (IKZ) and will open up the possibility of further clarifying and evaluating the potential for future β-$(Al_xGa_{1-x})_2O_3$ device applications.

TABLE I. Material properties of β-Ga_2O_3 and β-$(Al_xGa_{1-x})_2O_3$ alloy with $x = 0.25$ and $x = 0.5$. Bandgaps of $x = 0.25$ and $x = 0.5$ are estimated from Refs. 35 and 36. The electron mobility limit for β-Ga_2O_3 is taken from Ref. 31, whereas the electron mobility ranges for $x = 0.25$ and $x = 0.5$ are taken from Ref. 37, respectively. The breakdown field strength is calculated using the empirical relationship in Ref. 38. The relative dielectric constant for β-Ga_2O_3 is taken from Ref. 39 and for Al_2O_3 from Ref. 40. The relative dielectric constants for $x = 0.25$ and $x = 0.5$ are estimated from 25% to 50% of the difference between the relative dielectric constant values for β-Ga_2O_3 and Al_2O_3. The calculation of BFOM is based on Ref. 41.

	β-Ga_2O_3	β-$(Al_{0.25}Ga_{0.75})_2O_3$	β-$(Al_{0.5}Ga_{0.5})_2O_3$
Bandgap E_g (eV)	4.6–4.8	5.0–5.2	5.6–5.8
Electron mobility μ ($cm^2\ V^{-1}\ s^{-1}$)	200	104	81
Breakdown field E_{br} (MV cm^{-1})	7.9–8.7	9.7–10.7	10.0–10.7
Relative dielectric constant ε	11.2	10.6	10.0
BFOM $\varepsilon\mu E_{br}^3$	2430–3340	2240–3000	3840–5000

Deposition and properties of β-Ga_2O_3 thin films

To produce the discussed electrically functional part of the device, homoepitaxial and heteroepitaxial β-Ga_2O_3 growth have been demonstrated using various deposition methods such as molecular beam epitaxy[48–53] (MBE), halide vapor phase epitaxy[54–56] (HVPE), pulsed laser deposition[57–59] (PLD), atomic layer deposition[60,61] (ALD), or metal-organic vapor phase epitaxy[62–73] (MOVPE). Over the last few years, an extensive research effort led to an enormous improvement in the material quality and transport properties of β-Ga_2O_3 thin films grown by MOVPE.[62–77] Its ability to achieve high growth rates at moderate chamber pressures and temperatures while maintaining high crystalline qualities represents a major advantage of MOVPE compared to other growth techniques such as MBE. Although MBE exhibits a less complex growth environment than MOVPE, extremely low growth rates ($<0.5\ \mu m\ h^{-1}$) due to limited evaporation of the metal source[48,49] and the formation of the Ga_2O volatile suboxide during growth[52] as well as the restricted deposition area and the requirement for ultra-high vacuum (UHV) limit its application on an industrial level. To date, HVPE dominates the growth of β-Ga_2O_3 thick layers for vertical power devices since it allows to grow β-Ga_2O_3 films at relatively fast growth rates $>10\ \mu m\ h^{-1}$.[78,79] However, extremely high growth rates typically result in layers with high surface roughness and high density of pits[55] and, therefore, require a polishing process step prior to device fabrication,[54] making an application on an industrial scale unfeasible. MOVPE growth rates with up to $3\ \mu m\ h^{-1}$ while maintaining a high crystalline quality have recently been demonstrated,[73] turning MOVPE into the leading method in realizing mass production of future β-Ga_2O_3 high-power devices.

Comprehensive growth studies have shown that high-quality homoepitaxial β-Ga_2O_3 thin films can be achieved within a wide MOVPE growth window using temperatures ranging from 600 to 950 °C and chamber pressures between 10 and 80 Torr as well as various VI/III ratios ranging between 200 and 10 000.[63,65,67,69–71,73,75,80] The majority of the experimental research has thereby focused on homoepitaxial growth on (100)[63,65–67]- and (010)[70,71,80,81]-oriented β-Ga_2O_3 substrates using tetraethylgallium (TEGa) as metal-organic (MO) precursor and pure oxygen as oxidant source, since they enable comparatively easy thin-film growth with smooth morphologies and high crystallinity.

Stable and controllable n-type doping using different group IV elements (Si,[63,67,70–72,80] Sn,[82,83] and Ge[75]) with carrier densities ranging between mid-10^{15} and $10^{20}\ cm^{-3}$ has successfully been demonstrated. Si is considered as the most efficient dopant candidate for MOVPE growth of β-Ga_2O_3, mainly resulting from its ability for complete dopant incorporation and activation as well as its high doping

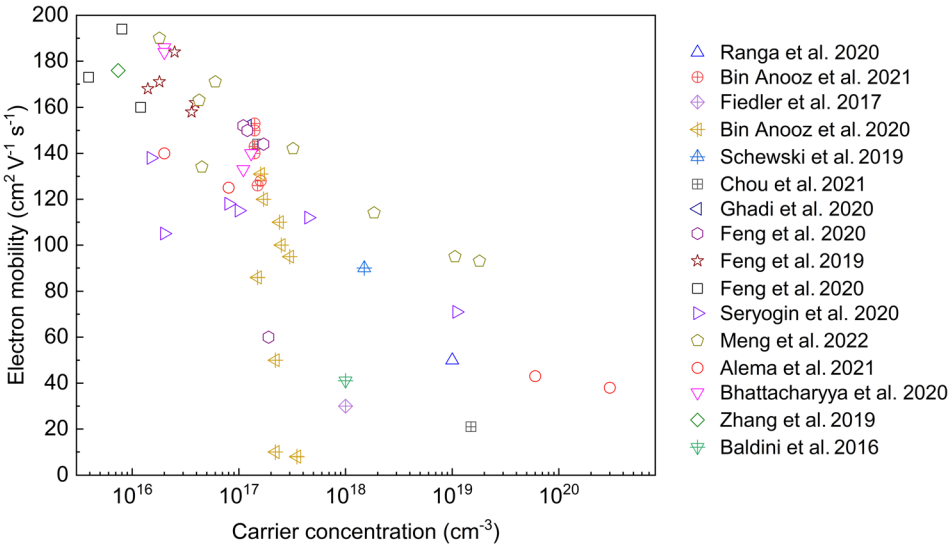

FIG. 2. Room-temperature Hall mobility vs carrier concentration for state-of-the-art MOVPE-grown β-Ga_2O_3 thin films on different substrate orientations (and miscut) using various n-type dopants and varying growth conditions.

efficiency and low memory effect in the reactor.[67,72,80] A Langmuir adsorption model has been proposed by Chou *et al.*[84] to reveal the competitive adsorption process between Ga and Si adsorption on the Ga lattice site, resulting in a growth rate-dependent doping behavior.

High room-temperature electron mobility of 194 $cm^2\ V^{-1}\ s^{-1}$ with a corresponding free carrier concentration of $8 \times 10^{15}\ cm^{-3}$ has already been demonstrated for MOVPE-grown Si-doped (010) β-Ga_2O_3,[71] which approaches the predicted theoretical limit of approximately 200 $cm^2\ V^{-1}\ s^{-1}$.[31] An overview of the room-temperature mobility vs carrier concentration of reported state-of-the-art MOVPE-grown β-Ga_2O_3 thin films is shown in Fig. 2.[10,63–73,75,80–82]

Although higher electron mobilities have been reported for MOVPE β-Ga_2O_3 thin films grown on (010) substrates compared to other orientations so far, the layers typically show a rougher surface morphology mainly caused by the formation of (110) and (–110) facets along the [001] direction during growth.[72,77,85,86] The faceting of the growth surface appears to be independent of the deposition method and has also been reported for (010) β-Ga_2O_3 layers grown via MBE.[51,53] However, (100) is the plane with the lowest surface energy[62] and the least density of surface states, which leads to a low trap density at the gate dielectric interface. Additionally, (100) substrates are more mechanically stable compared to (010)-oriented substrates; therefore, device separation at the end of the process chain is expected to be easier due to suppressed unintentional cleaving. Furthermore, step-flow growth at high growth rates resulting in layers with low surface roughness and high crystalline quality for thicknesses up to 3 μm has already been demonstrated[67] and, therefore, turns the (100) plane into the favorable substrate orientation for future power electronics requiring high crystalline quality, high electron mobilities, and low doping densities.

HOMOEPITAXIAL (100) β-Ga_2O_3 THIN FILMS VIA MOVPE FOR POWER ELECTRONIC APPLICATIONS

Even though the (100) plane is the preferred cleavage plane of β-Ga_2O_3 with the lowest surface energy and is easy to be prepared,[62,87] previous studies have shown that homoepitaxial layers grown on substrates with no intentional miscut (<0.3°) suffer from a high density of twins and stacking faults[88] in the grown layer due to the double positioning of Ga adatoms[62] on the (100) plane. These structural defects harm the electrical properties of the grown film since they compensate for the n-type doping and significantly reduce the carrier mobility. This defect formation is mainly induced by the nucleation of 2D islands on the (100) plane, resulting from limited effective diffusion lengths of Ga adatoms during growth.[62,66]

As shown in Fig. 3(a), the transmission electron microscopy (TEM) analysis reveals the presence of a high density of planar defects from a layer grown on a low miscut substrate (~0.5°), and these defects turn out to be twin lamellae,[64] which can be described by a c/2

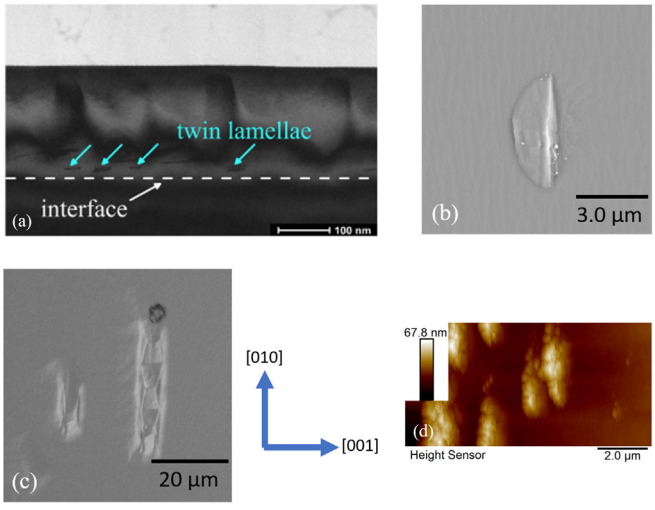

FIG. 3. The twin lamellae are characterized by (a) a cross-sectional TEM image, (b) an SEM image, (c) a light microscopy image, and (d) an AFM image. Figure (a) is reproduced with permission from Bin Anooz *et al.*, Appl. Phys. Lett. **116**, 182106 (2020). Copyright 2020 AIP Publishing.

glide reflection of the monoclinic lattice. Such twin lamellae can penetrate through the whole layer and end up on the surface,[62] making them even visible under scanning electron microscopy (SEM) and light microscopy, as shown in Figs. 3(b) and 3(c), respectively. The observed twin lamellae are bulk defects with an 2 to 5 μm long axis along the (010) direction, and the height of the defect out of the substrate surface is around 50 to 100 nm, as shown under the atomic force microscope (AFM) in Fig. 3(d). Most twin defects were formed inside the epilayer, while the substrate was free of structural defects.[89,90] Two major issues are observed with the existence of structural defects in the layers: (1) mobility collapse and (2) inhomogeneous electrical properties. For the issue of mobility collapse, the carrier mobility is measurable only in layers with electron concentration above $>1 \times 10^{18}\,\mathrm{cm}^{-3}$, and the measured carrier mobilities are between 30 and $10\,\mathrm{cm}^2\,\mathrm{V}^{-1}\,\mathrm{s}^{-1}$, which are quantitatively lower than the theoretical calculation[31] by one order of magnitude. The layers are still conductive for the electron concentration $<1 \times 10^{18}\,\mathrm{cm}^{-3}$, but the carrier mobility is not measurable. A similar mobility collapse is reported in the GaN system and is explained by the presence of potential barriers due to a high density of dislocations.[91,92] For the inhomogeneous electrical properties, the four-terminal resistances of the van der Pauw measurement show a ten-times higher resistance along the (001) direction than the (010) direction, which is not expected since the electron transport properties of β-Ga_2O_3 have been shown to be almost isotropic.[93] This anisotropic resistance can, thus, be related to the structure of the twin lamellae mentioned above since the long axis of the twin lamellae is perpendicular to the (001) direction.

The mechanism of twin lamellae formation has been studied in early work on epitaxial growth by Hall *et al.*[94] and Dickson *et al.*[95] In the case of a proper surface misorientation, the adatoms are able to reach the nearest step edge easier if their effective diffusion length is comparable to the surface terraces width, which inhibits the formation of twin lamellae through double positioning. On the other hand, if the effective diffusion length is shorter than the terrace width, the twin lamellae formation is promoted due to island nucleation on the growth terrace. A quantitative model that describes the formation of twin lamellae through double positioning has been presented by Schewski *et al.*[62] With the above understanding, the correlation among the surface morphology, the effective diffusion length, and the surface terrace width can be established based on the substrate misorientation and the growth conditions. Three typical surface morphologies are usually observed under AFM [Fig. 4(a)]:[65] 2D islands growth, step-flow, and step-bunching. Among all morphologies, the step-flow morphology morphology has the lowest density of defects, as revealed by TEM investigations [Fig. 4(b)], which makes it highly desirable in MOVPE-grown β-Ga_2O_3. However, step-flow growth mode can only be obtained when the effective diffusion length of the adatoms corresponds to the terrace width of the substrate surface. For such a purpose, applying a higher substrate misorientation is an intuitive solution, but it conflicts with the principle of sustainable development due to a more considerable

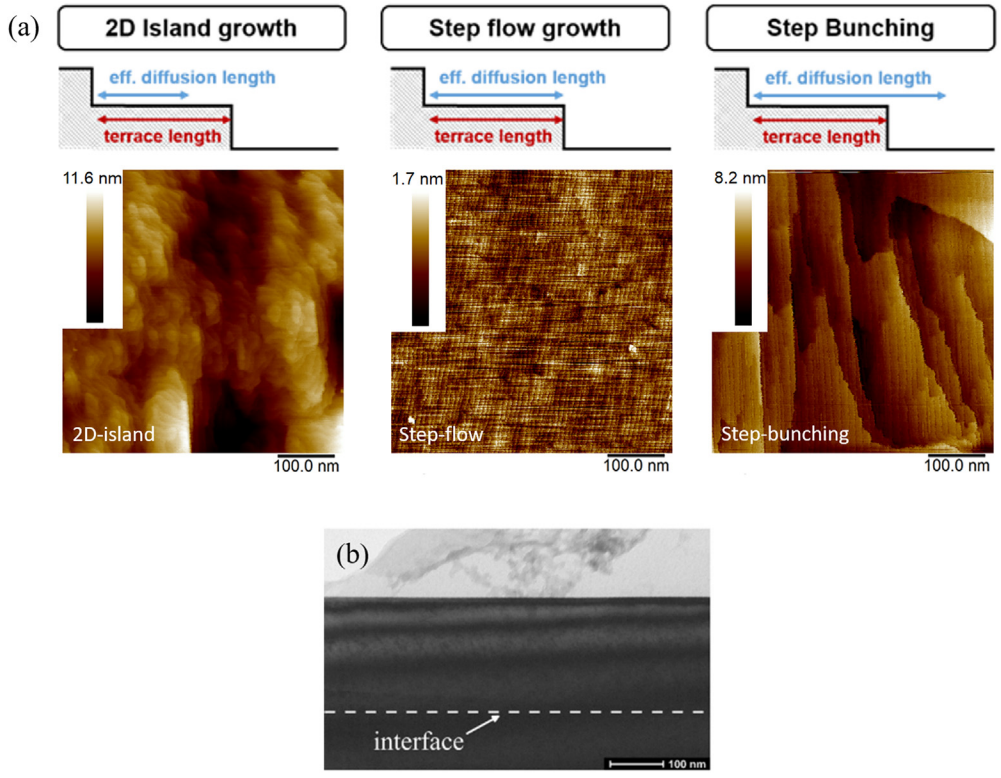

FIG. 4. (a) Scheme of the correlation between surface morphology, the effective surface diffusion length and the surface terrace width, and the corresponding AFM image of each morphology: 2D islands growth, step-flow, and step-bunching. (b) TEM image of a β-Ga_2O_3 layer which showed step-flow morphology under AFM. The TEM image is reproduced with permission from Anooz *et al.*, Appl. Phys. Lett. **116**, 182106 (2020). Copyright 2020 AIP Publishing.

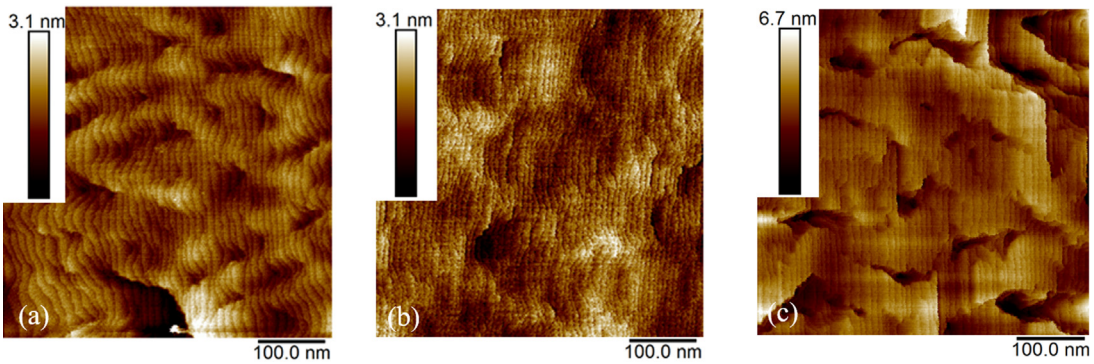

FIG. 5. AFM images of homoepitaxial (100) β-Ga_2O_3 thin films with step-flow morphology under the growth condition of Ref. 67 and different film thicknesses: (a) 0.3, (b) 3, and (c) 4 μm. Figures (a) and (b) are reproduced with permission from Chou *et al.*, AIP Adv. **11**, 115323 (2021). Copyright 2021 AIP Publishing.

material loss. Therefore, prolonging the effective diffusion length of Ga adatoms by finding a proper growth window is another approach to achieve the desired step-flow growth mode.

A well-controlled VI/III ratio has also been shown experimentally to be a critical factor to control the surface morphology of the MOVPE-grown layer. An increase in the Ga flux and a decrease in the VI/III ratio increase the effective diffusion length of the Ga adatoms, enabling step-flow growth to be maintained at various miscut angles, i.e., 2°, 4°, and 6°. Growth on the substrates with 4° and 2° miscut resulted in RT Hall mobilities of 131 and 120 $cm^2\ V^{-1}\ s^{-1}$, respectively. A record RT Hall mobility of 153 $cm^2\ V^{-1}\ s^{-1}$ with a free carrier concentration of $1.4 \times 10^{17}\ cm^{-3}$ for Si-doped (100) β-Ga_2O_3 with a miscut of 4° and a film thickness of 300 nm was achieved,[63] and a lateral MOSFET structure based on such films has been successfully demonstrated with a breakdown voltage around 1200 V, which is equivalent to an average breakdown field strength of 2 MV cm^{-1}.[20] Kinetic Monte Carlo (KMC)[96] simulation also suggested that the oxygen amount plays an important role in morphology control. Once oxygen atoms are attached to the Ga adatoms on the surface, the activation energy for a motion of Ga adatoms becomes much higher, and the nucleation is much easier to happen on the surface terrace instead of the step edge, resulting in undesired 2D island growth.

The chamber pressure is another critical growth parameter that implicitly but significantly influences the VI/III ratio during the growth and thereby the surface roughness of the grown samples, which is reported in both (100)[63] and (010)[71] β-Ga_2O_3 thin films. Since the growth window mostly reported for MOVPE-grown β-Ga_2O_3 thin films is in the mass-transport-limited regime (the growth rate increases linearly with the increase in Ga precursor concentrations), the chamber pressure is believed to be critical for the transport mechanism of the gaseous precursors in the chamber. It is observed that a higher chamber pressure shortens the effective diffusion length of adatoms and results in a morphology transition from step-flow to 2D-island growth with a decrease in the thin-film growth rate simultaneously. On the other hand, a lower chamber pressure transits the surface morphology from step-flow to step-bunching and increases the thin-film growth rate while keeping the other parameters fixed. Similar observations regarding the influence of the chamber pressure have also been made by layers grown on (010) oriented substrates.[71,74]

However, to fulfill the requirement for the vertical device structure, a homoepitaxial drift layer with a thickness of several micrometers grown on conductive substrates should be achieved. Together with the recent development of the conductive β-Ga_2O_3 bulk crystal,[97] a significant enhancement of the epitaxial film thickness up to 3 μm and a growth rate above 1 $\mu m\ h^{-1}$ was demonstrated by lowering the VI/III ratio to the boundary of O-rich and Ga-rich growth conditions,[67] while a step-flow morphology resulting in a smooth surface roughness (RMS < 1.0 nm) has been maintained for various film thicknesses, as shown in Figs. 5(a)–5(c). It seems that the growth environment under a lower VI/III ratio results in a more stable Ga wetting layer (or Ga adlayer), stabilizing the surface morphology during growth. Just like the adlayer mechanism reported in the GaN system,[98–100] the reduction in the VI/III ratio has significantly affected the effective diffusion length of Ga adatoms on the (100) β-Ga_2O_3 surface during film growth. A similar result has been reported by Okamura *et al.*[101] for smooth (010) β-Ga_2O_3 films grown by MBE, where step-flow growth was also attributed to the slight Ga-rich growth window together with a 2° substrate miscut along the (001) direction, and a similar diffusion-enhanced mechanism was proposed.

OUTLOOK OF (100) β-Ga_2O_3 TOWARD POWER ELECTRONICS APPLICATION

Achieving β-Ga_2O_3 films with smooth surface morphologies at high thicknesses and excellent electrical properties is crucial for developing high-performance power electronic devices, and it is an ongoing work in the community. Many researchers have already reported as-grown films with high mobility and low compensator concentration. However, challenges remain in obtaining a smooth surface (both microscopically and macroscopically) at a high thickness (>3 μm) while maintaining good electrical properties. For the microscopic smoothness, the smoothest surface at a thickness above 3 μm is demonstrated for the (100) orientation (RMS < 0.5 nm) due to its step-flow growth mode on the intentionally misoriented substrate.[67] On the other hand, the (010) orientation, due to its facet growth mode whose coalescence results in the formation of trenches, the film roughness is usually in the range of 1–2 nm, and it tends to get even rougher with further increase in thickness or growth rate.[73] Mazzolini *et al.*[53] and Okumura *et al.*[101] have demonstrated smooth (010) films grown by MBE where step-flow growth was dominated and attributed to an

offcut along the [001] direction. The above observations motivate to gain a further understanding of the optimal substrate geometry and wafer flat specifications for (100) and (010) β-Ga_2O_3 substrates and all other potential orientations. However, since both (100) and (010) substrates contain cleavage planes, any stress applied during the grinding, polishing and misorientation treatment might induce self-cleavage requiring proper treatment strategies. For the macroscopic smoothness, it has been observed that a large number of parasitic particles start to appear on the grown film surface when the thickness increases above 3 μm. Such particles might be potential compensators and even induce structural defects, which dramatically degrade the electrical performance of the thick layer and are the hindrance toward the growth of tens of μm-thick films. At the current stage, 3.2 μm thickness is the highest value reported for MOVPE-grown β-Ga_2O_3 films regardless of the orientation. An upcoming report from our side will address more details of parasitic particle formation and the optimization approach.

Moreover, for the development of the MOVPE process, the growth of an epitaxial (thin) film is an implicit function of many process parameters, which results in high-dimensional parameter space. Searching for the optimized parameter combination is extremely time-consuming and comes with a high cost of resources and labor. Recent works have demonstrated the potential of implementing the machine learning approach to investigate the thin-film growth rate[102] as well as the doping level[103] of MOVPE-grown (100) β-Ga_2O_3 thin films using real experimental datasets. It has been demonstrated that the algorithms like Random Forest[104] can assess the non-linear relation and the importance of the growth parameters. By training such a model, one can explore the parameter space of the growth technique by focusing on the critical parameters, which show a strong correlation with the desired properties. In addition, one can also, based on domain knowledge, create new artificial parameters (e.g., the ratio between different growth parameters) to verify the hypothesis via estimating the influence of the newly added parameter, and new insight into the growth process and the observed mechanism might be found.[84] Such a data-driven approach can be a powerful tool to speed up the development cycle of material growth, which is not limited to the MOVPE process.

In addition to the immense study of homoepitaxial grown β-Ga_2O_3 thin films, modulation doping of β-$(Al_xGa_{1-x})_2O_3$ barrier layers in β-$(Al_xGa_{1-x})_2O_3$/Ga_2O_3 heterostructure field effect transistors (FETs) is predicted to show a significant enhancement in the device performance compared to conventional β-Ga_2O_3-based devices. To realize its promised potentials, the challenges of phase segregation and nonuniform distribution at high Al content need to be addressed, and a profound understanding of the influence of the growth condition on electrical properties of MOVPE-grown β-$(Al_xGa_{1-x})_2O_3$ alloys is the key interest. It has been shown recently that crystal orientation plays an important role in the Al incorporation limit and band offsets, and (100) orientation is predicted to be the promising orientation to have the highest critical thickness[105] and incorporated Al content.[36,46] The potential role of off-oriented (100) β-Ga_2O_3 substrates is suggested to achieve the full advantage of β-$(Al_xGa_{1-x})_2O_3$/Ga_2O_3 heterostructures with the benefit of suppressing the formation of twin defects as reported in Ref. 46, and the same benefit might be acquired by all other preferential orientations with proper off-orientation. Finally, the successful development of high-quality β-$(Al_xGa_{1-x})_2O_3$ single crystal substrates will allow one to achieve homoepitaxial thin films with a higher crystalline quality for varying Al compositions and will enable the next step in further going down the road in the realization of future high-power electronics.

In summary, we have reviewed the electrical, structural, and growth development of MOVPE-grown β-Ga_2O_3 with the aim of demonstrating the power device prototype in vertical and lateral architecture. The current endeavors of growing high-quality β-Ga_2O_3 films have been demonstrated by introducing the (100) substrate orientation and exploring the new growth window to reach the epitaxy requirement for the high-voltage sustainable device. Following the review of the development path and the recent results, we identified the solved challenges and the remaining issues and depicted the future perspectives of β-Ga_2O_3 based on the learned experience. The β-Ga_2O_3-based power device and its alloys have great potential for next-generation high-power and radio frequency electronic applications for electric vehicles, power conversion, satellite communication, radar, and wireless infrastructure.

ACKNOWLEDGMENTS

This work was performed in the framework of GraFOx, a Leibniz ScienceCampus. The work was funded by the BMBF under Grant No. 16ES1084K, the European Community (Europäische Fonds für regionale Entwicklung-EFRE) under Grant No. 1.8/15, and by the Deutsche Forschungsgemeinschaft under project funding Reference No. PO-2659/1-2.

AUTHOR DECLARATIONS

Conflict of Interest

The authors have no conflicts to disclose.

Author Contributions

Jana Rehm and Ta-Shun Chou contributed equally to this work.

Jana Rehm: Conceptualization (lead); Writing – original draft (lead). **Ta-Shun Chou:** Conceptualization (lead); Writing – original draft (lead). **Saud Bin Anooz:** Conceptualization (equal); Writing – review & editing (equal). **Palvan Seyidov:** Conceptualization (supporting); Writing – review & editing (supporting). **Andreas Fiedler:** Conceptualization (supporting); Writing – review & editing (supporting). **Zbigniew Galazka:** Conceptualization (supporting); Writing – review & editing (supporting). **Andreas Popp:** Conceptualization (equal); Funding acquisition (lead); Project administration (lead); Writing – review & editing (lead).

DATA AVAILABILITY

The data that support the findings of this study are available from the corresponding author upon reasonable request.

REFERENCES

[1]B. K. Bose, IEEE Trans. Ind. Electron. **60**, 2638 (2013).
[2]A. J. Green, J. Speck, G. Xing, P. Moens, F. Allerstam, K. Gumaelius, T. Neyer, A. Arias-Purdue, V. Mehrotra, A. Kuramata, K. Sasaki, S. Watanabe, K. Koshi, J. Blevins, O. Bierwagen, S. Krishnamoorthy, K. Leedy, A. R. Arehart, A. T. Neal, S. Mou, S. A. Ringel, A. Kumar, A. Sharma, K. Ghosh, U.

Singisetti, W. Li, K. Chabak, K. Liddy, A. Islam, S. Rajan, S. Graham, S. Choi, Z. Cheng, and M. Higashiwaki, APL Mater. **10**, 029201 (2022).
[3]M. Higashiwaki and G. H. Jessen, Appl. Phys. Lett. **112**, 060401 (2018).
[4]M. Higashiwaki, A. Kuramata, H. Murakami, and Y. Kumagai, J. Phys. D **50**, 333002 (2017).
[5]B. J. Baliga, J. Appl. Phys. **53**, 1759 (1982).
[6]M. Higashiwaki, K. Sasaki, A. Kuramata, T. Masui, and S. Yamakoshi, Phys. Status Solidi A **211**, 21 (2014).
[7]X. Cheng, IOP Conf. Ser. **439**, 022033 (2018).
[8]M. Higashiwaki, H. Murakami, Y. Kumagai, and A. Kuramata, Jpn. J. Appl. Phys. **55**, 1202A1 (2016).
[9]S. B. Reese, T. Remo, J. Green, and A. Zakutayev, Joule **3**, 903 (2019).
[10]P. Ranga, A. Bhattacharyya, A. Chmielewski, S. Roy, N. Alem, and S. Krishnamoorthy, Appl. Phys. Lett. **117**, 172105 (2020).
[11]Z. Galazka, R. Uecker, D. Klimm, K. Irmscher, M. Naumann, M. Pietsch, A. Kwasniewski, R. Bertram, S. Ganschow, and M. Bickermann, ECS J. Solid State Sci. Technol. **6**, Q3007 (2017).
[12]Z. Galazka, J. Appl. Phys. **131**, 031103 (2022).
[13]A. Kuramata, K. Koshi, S. Watanabe, Y. Yamaoka, T. Masui, and S. Yamakoshi, Jpn. J. Appl. Phys. **55**, 1202A2 (2016).
[14]K. Hoshikawa, T. Kobayashi, Y. Matsuki, E. Ohba, and T. Kobayashi, J. Cryst. Growth **545**, 125724 (2020).
[15]K. Hoshikawa, E. Ohba, T. Kobayashi, J. Yanagisawa, C. Miyagawa, and Y. Nakamura, J. Cryst. Growth **447**, 36 (2016).
[16]M. A. Mastro, A. Kuramata, J. Calkins, J. Kim, F. Ren, and S. J. Pearton, ECS J. Solid State Sci. Technol. **6**, P356 (2017).
[17]K. D. Chabak, K. D. Leedy, A. J. Green, S. Mou, A. T. Neal, T. Asel, E. R. Heller, N. S. Hendricks, K. Liddy, A. Crespo, N. C. Miller, M. T. Lindquist, N. A. Moser, R. C. Fitch, D. E. Walker, D. L. Dorsey, and G. H. Jessen, Semicond. Sci. Technol. **35**, 013002 (2020).
[18]M. Ogita, N. Saika, Y. Nakanishi, and Y. Hatanaka, Appl. Surf. Sci. **142**, 188 (1999).
[19]K. Tetzner, E. B. Treidel, O. Hilt, A. Popp, S. B. Anooz, G. Wagner, A. Thies, K. Ickert, H. Gargouri, and J. Würfl, IEEE Electron Device Lett. **40**, 1503 (2019).
[20]K. Tetzner, O. Hilt, A. Popp, S. Bin Anooz, and J. Würfl, Microelectron. Reliab. **114**, 113951 (2020).
[21]M. Higashiwaki, K. Sasaki, A. Kuramata, T. Masui, and S. Yamakoshi, Appl. Phys. Lett. **100**, 013504 (2012).
[22]M. H. Wong, K. Sasaki, A. Kuramata, S. Yamakoshi, and M. Higashiwaki, Jpn. J. Appl. Phys. **55**, 1202B9 (2016).
[23]M. H. Wong, K. Sasaki, A. Kuramata, S. Yamakoshi, and M. Higashiwaki, IEEE Electron Device Lett. **37**, 212 (2016).
[24]E. Farzana, F. Alema, W. Y. Ho, A. Mauze, T. Itoh, A. Osinsky, and J. S. Speck, Appl. Phys. Lett. **118**, 162109 (2021).
[25]Z. Xia, H. Chandrasekar, W. Moore, C. Wang, A. J. Lee, J. McGlone, N. K. Kalarickal, A. Arehart, S. Ringel, F. Yang, and S. Rajan, Appl. Phys. Lett. **115**, 252104 (2019).
[26]B. Chatterjee, Y. Song, J. S. Lundh, Y. Zhang, Z. Xia, Z. Islam, J. Leach, C. McGray, P. Ranga, S. Krishnamoorthy, A. Haque, S. Rajan, and S. Choi, Appl. Phys. Lett. **117**, 153501 (2020).
[27]J. B. Varley, A. Perron, V. Lordi, D. Wickramaratne, and J. L. Lyons, Appl. Phys. Lett. **116**, 172104 (2020).
[28]S. Krishnamoorthy, Z. Xia, C. Joishi, Y. Zhang, J. McGlone, J. Johnson, M. Brenner, A. R. Arehart, J. Hwang, S. Lodha, and S. Rajan, Appl. Phys. Lett. **111**, 023502 (2017).
[29]Y. Zhang, A. Neal, Z. Xia, C. Joishi, J. M. Johnson, Y. Zheng, S. Bajaj, M. Brenner, D. Dorsey, K. Chabak, G. Jessen, J. Hwang, S. Mou, J. P. Heremans, and S. Rajan, Appl. Phys. Lett. **112**, 173502 (2018).
[30]P. Ranga, A. Rishinaramangalam, J. Varley, A. Bhattacharyya, D. Feezell, and S. Krishnamoorthy, Appl. Phys. Express **12**, 111004 (2019).
[31]N. Ma, N. Tanen, A. Verma, Z. Guo, T. Luo, H. Xing, and D. Jena, Appl. Phys. Lett. **109**, 212101 (2016).
[32]P. Ranga, A. Bhattacharyya, A. Chmielewski, S. Roy, R. Sun, M. A. Scarpulla, N. Alem, and S. Krishnamoorthy, Appl. Phys. Express **14**, 025501 (2021).
[33]P. Ranga, A. Bhattacharyya, A. Rishinaramangalam, Y. K. Ooi, M. A. Scarpulla, D. Feezell, and S. Krishnamoorthy, Appl. Phys. Express **13**, 045501 (2020).
[34]A. F. M. A. U. Bhuiyan, Z. Feng, J. M. Johnson, H.-L. Huang, J. Sarker, M. Zhu, M. R. Karim, B. Mazumder, J. Hwang, and H. Zhao, APL Mater. **8**, 031104 (2020).
[35]H. Peelaers, J. B. Varley, J. S. Speck, and C. G. van de Walle, Appl. Phys. Lett. **112**, 242101 (2018).
[36]A. F. M. Anhar Uddin Bhuiyan, Z. Feng, J. M. Johnson, H.-L. Huang, J. Hwang, and H. Zhao, Appl. Phys. Lett. **117**, 252105 (2020).
[37]X. Duan, T. Wang, Z. Fu, J.-Y. Yang, and L. Liu, Appl. Phys. Lett. **121**, 042103 (2022).
[38]J. L. Hudgins, G. S. Simin, E. Santi, and M. A. Khan, IEEE Trans. Power Electron. **18**, 907 (2003).
[39]A. Fiedler, R. Schewski, Z. Galazka, and K. Irmscher, ECS J. Solid State Sci. Technol. **8**, Q3083 (2019).
[40]J. B. Varley, J. Mater. Res. **36**, 4790 (2021).
[41]B. J. Baliga, IEEE Electron Device Lett. **10**, 455 (1989).
[42]A. F. M. A. U. Bhuiyan, Z. Feng, J. M. Johnson, Z. Chen, H.-L. Huang, J. Hwang, and H. Zhao, Appl. Phys. Lett. **115**, 120602 (2019).
[43]A. F. M. A. U. Bhuiyan, Z. Feng, L. Meng, A. Fiedler, H.-L. Huang, A. T. Neal, E. Steinbrunner, S. Mou, J. Hwang, S. Rajan, and H. Zhao, J. Appl. Phys. **131**, 145301 (2022).
[44]J. M. Johnson, H.-L. Huang, M. Wang, S. Mu, J. B. Varley, A. F. M. A. Uddin Bhuiyan, Z. Feng, N. K. Kalarickal, S. Rajan, H. Zhao, C. G. Van de Walle, and J. Hwang, APL Mater. **9**, 051103 (2021).
[45]A. F. M. Anhar Uddin Bhuiyan, Z. Feng, J. M. Johnson, H.-L. Huang, J. Hwang, and H. Zhao, Appl. Phys. Lett. **117**, 142107 (2020).
[46]A. F. M. Anhar Uddin Bhuiyan, Z. Feng, J. M. Johnson, H.-L. Huang, J. Hwang, and H. Zhao, Cryst. Growth Des. **20**, 6722 (2020).
[47]A. F. M. A. U. Bhuiyan, Z. Feng, L. Meng, and H. Zhao, J. Mater. Res. **36**, 4804 (2021).
[48]E. Ahmadi, O. S. Koksaldi, S. W. Kaun, Y. Oshima, D. B. Short, U. K. Mishra, and J. S. Speck, Appl. Phys. Express **10**, 041102 (2017).
[49]K. Sasaki, A. Kuramata, T. Masui, E. G. Víllora, K. Shimamura, and S. Yamakoshi, Appl. Phys. Express **5**, 035502 (2012).
[50]M.-Y. Tsai, O. Bierwagen, M. E. White, and J. S. Speck, J. Vac. Sci. Technol. A **28**, 354 (2010).
[51]P. Mazzolini, P. Vogt, R. Schewski, C. Wouters, M. Albrecht, and O. Bierwagen, APL Mater. **7**, 022511 (2019).
[52]P. Vogt and O. Bierwagen, Appl. Phys. Lett. **108**, 072101 (2016).
[53]P. Mazzolini and O. Bierwagen, J. Phys. D **53**, 354003 (2020).
[54]K. Goto, K. Konishi, H. Murakami, Y. Kumagai, B. Monemar, M. Higashiwaki, A. Kuramata, and S. Yamakoshi, Thin Solid Films **666**, 182 (2018).
[55]H. Murakami, K. Nomura, K. Goto, K. Sasaki, K. Kawara, Q. T. Thieu, R. Togashi, Y. Kumagai, M. Higashiwaki, A. Kuramata, S. Yamakoshi, B. Monemar, and A. Koukitu, Appl. Phys. Express **8**, 015503 (2015).
[56]K. Nomura, K. Goto, R. Togashi, H. Murakami, Y. Kumagai, A. Kuramata, S. Yamakoshi, and A. Koukitu, J. Cryst. Growth **405**, 19 (2014).
[57]Y. An, L. Dai, Y. Wu, B. Wu, Y. Zhao, T. Liu, H. Hao, Z. Li, G. Niu, J. Zhang, Z. Quan, and S. Ding, J. Adv. Dielectr. **09**, 1950032 (2019).
[58]X. H. Chen, S. Han, Y. M. Lu, P. J. Cao, W. J. Liu, Y. X. Zeng, F. Jia, W. Y. Xu, X. K. Liu, and D. L. Zhu, J. Alloys Compd. **747**, 869 (2018).
[59]K. D. Leedy, K. D. Chabak, V. Vasilyev, D. C. Look, J. J. Boeckl, J. L. Brown, S. E. Tetlak, A. J. Green, N. A. Moser, A. Crespo, D. B. Thomson, R. C. Fitch, J. P. McCandless, and G. H. Jessen, Appl. Phys. Lett. **111**, 012103 (2017).
[60]D.-W. Choi, K.-B. Chung, and J.-S. Park, Thin Solid Films **546**, 31 (2013).
[61]Dezelah, J. Niinistö, K. Arstila, L. Niinistö, and C. H. Winter, Chem. Mater. **18**, 471 (2006).
[62]R. Schewski, M. Baldini, K. Irmscher, A. Fiedler, T. Markurt, B. Neuschulz, T. Remmele, T. Schulz, G. Wagner, Z. Galazka, and M. Albrecht, J. Appl. Phys. **120**, 225308 (2016).
[63]S. Bin Anooz, R. Grüneberg, T. S. Chou, A. Fiedler, K. Irmscher, C. Wouters, R. Schewski, M. Albrecht, Z. Galazka, W. Miller, J. Schwarzkopf, and A. Popp, J. Phys. D **54**, 034003 (2021).
[64]A. Fiedler, R. Schewski, M. Baldini, Z. Galazka, G. Wagner, M. Albrecht, and K. Irmscher, J. Appl. Phys. **122**, 165701 (2017).
[65]S. Bin Anooz, R. Grüneberg, C. Wouters, R. Schewski, M. Albrecht, A. Fiedler, K. Irmscher, Z. Galazka, W. Miller, G. Wagner, J. Schwarzkopf, and A. Popp, Appl. Phys. Lett. **116**, 182106 (2020).

[66]R. Schewski, K. Lion, A. Fiedler, C. Wouters, A. Popp, S. V. Levchenko, T. Schulz, M. Schmidbauer, S. Bin Anooz, R. Grüneberg, Z. Galazka, G. Wagner, K. Irmscher, M. Scheffler, C. Draxl, and M. Albrecht, APL Mater. **7**, 022515 (2019).
[67]T.-S. Chou, P. Seyidov, S. B. Anooz, R. Grüneberg, T. T. V. Tran, K. Irmscher, M. Albrecht, Z. Galazka, J. Schwarzkopf, and A. Popp, AIP Adv. **11**, 115323 (2021).
[68]H. Ghadi, J. F. McGlone, C. M. Jackson, E. Farzana, Z. Feng, A. Bhuiyan, H. Zhao, A. R. Arehart, and S. A. Ringel, APL Mater. **8**, 021111 (2020).
[69]Z. Feng, A. F. M. Anhar Uddin Bhuiyan, N. K. Kalarickal, S. Rajan, and H. Zhao, Appl. Phys. Lett. **117**, 222106 (2020).
[70]Z. Feng, A. F. M. Anhar Uddin Bhuiyan, M. R. Karim, and H. Zhao, Appl. Phys. Lett. **114**, 250601 (2019).
[71]Z. Feng, A. F. M. Anhar Uddin Bhuiyan, Z. Xia, W. Moore, Z. Chen, J. F. McGlone, D. R. Daughton, A. R. Arehart, S. A. Ringel, S. Rajan, and H. Zhao, Phys. Status Solidi RRL **14**, 2000145 (2020).
[72]G. Seryogin, F. Alema, N. Valente, H. Fu, E. Steinbrunner, A. T. Neal, S. Mou, A. Fine, and A. Osinsky, Appl. Phys. Lett. **117**, 262101 (2020).
[73]L. Meng, Z. Feng, A. Bhuiyan, and H. Zhao, Cryst. Growth Des. **22**, 3896 (2022).
[74]F. Alema, B. Hertog, A. Osinsky, P. Mukhopadhyay, M. Toporkov, and W. V. Schoenfeld, J. Cryst. Growth **475**, 77 (2017).
[75]F. Alema, G. Seryogin, A. Osinsky, and A. Osinsky, APL Mater. **9**, 091102 (2021).
[76]F. Alema, Y. Zhang, A. Osinsky, N. Orishchin, N. Valente, A. Mauze, and J. S. Speck, APL Mater. **8**, 021110 (2020).
[77]F. Alema, Y. Zhang, A. Osinsky, N. Valente, A. Mauze, T. Itoh, and J. S. Speck, APL Mater. **7**, 121110 (2019).
[78]Z. Hu, K. Nomoto, W. Li, N. Tanen, K. Sasaki, A. Kuramata, T. Nakamura, D. Jena, and H. G. Xing, IEEE Electron Device Lett. **39**, 869 (2018).
[79]W. Li, K. Nomoto, Z. Hu, D. Jena, and H. G. Xing, IEEE Electron Device Lett. **41**, 107 (2020).
[80]A. Bhattacharyya, P. Ranga, S. Roy, J. Ogle, L. Whittaker-Brooks, and S. Krishnamoorthy, Appl. Phys. Lett. **117**, 142102 (2020).
[81]Y. Zhang, F. Alema, A. Mauze, O. S. Koksaldi, R. Miller, A. Osinsky, and J. S. Speck, APL Mater. **7**, 022506 (2019).
[82]M. Baldini, M. Albrecht, A. Fiedler, K. Irmscher, R. Schewski, and G. Wagner, ECS J. Solid State Sci. Technol. **6**, Q3040 (2017).
[83]M. Baldini, M. Albrecht, A. Fiedler, K. Irmscher, D. Klimm, R. Schewski, and G. Wagner, J. Mater. Sci. **51**, 3650 (2016).
[84]T.-S. Chou, S. B. Anooz, R. Grüneberg, N. Dropka, J. Rehm, T. T. V. Tran, K. Irmscher, P. Seyidov, W. Miller, Z. Galazka, M. Albrecht, and A. Popp, Appl. Phys. Lett. **121**, 032103 (2022).
[85]F. Alema, Y. Zhang, A. Mauze, T. Itoh, J. S. Speck, B. Hertog, and A. Osinsky, AIP Adv. **10**, 085002 (2020).
[86]R. Miller, F. Alema, and A. Osinsky, IEEE Trans. Semicond. Manuf. **31**, 467 (2018).
[87]P. Mazzolini, A. Falkenstein, C. Wouters, R. Schewski, T. Markurt, Z. Galazka, M. Martin, M. Albrecht, and O. Bierwagen, APL Mater. **8**, 011107 (2020).
[88]G. Wagner, M. Baldini, D. Gogova, M. Schmidbauer, R. Schewski, M. Albrecht, Z. Galazka, D. Klimm, and R. Fornari, Phys. Status Solidi A **211**, 27 (2014).
[89]Z. Galazka, S. Ganschow, K. Irmscher, D. Klimm, M. Albrecht, R. Schewski, M. Pietsch, T. Schulz, A. Dittmar, A. Kwasniewski, R. Grueneberg, S. B. Anooz, A. Popp, U. Juda, I. M. Hanke, T. Schroeder, and M. Bickermann, Prog. Cryst. Growth Charact. Mater. **67**, 100511 (2021).
[90]Z. Galazka, K. Irmscher, R. Uecker, R. Bertram, M. Pietsch, A. Kwasniewski, M. Naumann, T. Schulz, R. Schewski, D. Klimm, and M. Bickermann, J. Cryst. Growth **404**, 184 (2014).
[91]J. L. Farvacque, Z. Bougrioua, and I. Moerman, Phys. Rev. B **63**, 115202 (2001).
[92]D. C. Look and J. R. Sizelove, Phys. Rev. Lett. **82**, 1237 (1999).
[93]E. G. Víllora, K. Shimamura, Y. Yoshikawa, K. Aoki, and N. Ichinose, J. Cryst. Growth **270**, 420 (2004).
[94]M. J. Hall and M. W. Thompson, Br. J. Appl. Phys. **12**, 495 (1961).
[95]E. W. Dickson and P. W. Pashley, Philos. Mag. **7**, 1315 (1962).
[96]W. Miller, D. Meiling, R. Schewski, A. Popp, S. B. Anooz, and M. Albrecht, Phys. Rev. Res. **2**, 033170 (2020).
[97]Z. Galazka, S. Ganschow, P. Seyidov, K. Irmscher, M. Pietsch, T.-S. Chou, S. B. Anooz, R. Grueneberg, A. Popp, A. Dittmar, A. Kwasniewski, M. Suendermann, D. Klimm, T. Straubinger, T. Schroeder, and M. Bickermann, Appl. Phys. Lett. **120**, 152101 (2022).
[98]G. Koblmüller, J. Brown, R. Averbeck, H. Riechert, P. Pongratz, and J. S. Speck, Jpn. J. Appl. Phys. **44**, L906 (2005).
[99]J. Neugebauer, T. K. Zywietz, M. Scheffler, J. E. Northrup, H. Chen, and R. M. Feenstra, Phys. Rev. Lett. **90**, 056101 (2003).
[100]H. Zheng, M. H. Xie, H. S. Wu, and Q. K. Xue, Phys. Rev. B **77**, 045303 (2008).
[101]H. Okumura, M. Kita, K. Sasaki, A. Kuramata, M. Higashiwaki, and J. S. Speck, Appl. Phys. Express **7**, 095501 (2014).
[102]T.-S. Chou, S. Bin Anooz, R. Grüneberg, N. Dropka, W. Miller, T. T. V. Tran, J. Rehm, M. Albrecht, and A. Popp, J. Cryst. Growth **592**, 126737 (2022).
[103]T.-S. Chou, S. Bin Anooz, R. Grüneberg, K. Irmscher, N. Dropka, J. Rehm, T. T. V. Tran, W. Miller, P. Seyidov, M. Albrecht, and A. Popp, Crystals **12**, 8 (2021).
[104]L. Breiman, Mach. Learn. **45**, 5 (2001).
[105]S. Mu, M. Wang, H. Peelaers, and C. G. Van de Walle, APL Mater. **8**, 091105 (2020).